High-power short-pulse laser repetition rate improvement by adaptive wave front correction

B. Wattellier
Laboratoire pour l'Utilisation des Lasers Intenses, URM n°7605 CNRS-École Polytechnique-CEA-Université Paris VI, École Polytechnique, 91128 Palaiseau Cedex, France and Phasics, Campus de l'École Polytechnique, Bât. 404, 91128 Palaiseau Cedex, France

J. Fuchs[a)]
Laboratoire pour l'Utilisation des Lasers Intenses, URM n°7605 CNRS-École Polytechnique-CEA-Université Paris VI, École Polytechnique, 91128 Palaiseau Cedex, France, General Atomics, San Diego, California 92121, and Physics Department, MS-220, University of Nevada, Reno, Nevada 89557

J. P. Zou and K. Abdeli
Laboratoire pour l'Utilisation des Lasers Intenses, URM n°7605 CNRS-École Polytechnique-CEA-Université Paris VI, École Polytechnique, 91128 Palaiseau Cedex, France

C. Haefner
Physics Department, MS-220, University of Nevada, Reno, Nevada 89557
and Gesellschaft für Schwerionenforschung mbH, 64291 Darmstadt, Germany

H. Pépin
Laboratoire pour l'Utilisation des Lasers Intenses, URM n°7605 CNRS-École Polytechnique-CEA-Université Paris VI, École Polytechnique, 91128 Palaiseau Cedex, France

(Received 23 August 2004; accepted 5 September 2004; published 10 November 2004)

Dynamic wave front correction is applied before each shot on a 100 TW, 30 J/300 fs high power laser facility using an adaptive optics system. This system allows one to increase the repetition rate of high-energy lasers while maintaining excellent and constant beam focusability with a Strehl ratio >0.75 despite the amplifiers not being in thermal equilibrium. Best results in terms of highest Strehl ratio and intensities are obtained when locking the system on wave front sensing after pulse recompression. © *2004 American Institute of Physics.* [DOI: 10.1063/1.1819379]

I. INTRODUCTION

High-field science has been one of the most rapidly growing areas in physics of the last decades, opening fascinating and entirely new applications.[1] To name a few, high fields can produce bright x-ray sources as well as x-ray lasers, they can accelerate particles to high energies ($\sim$1 GeV) over microns of distance only, or produce high-energy density matter as well as allow lidars to work in a wider, broadband mode. All these applications rely on achieving the highest amplitude electric fields. This is done primarily by focusing a short-pulse laser in the 10 TW–1 PW range that is produced by the chirped pulse amplification (CPA) technique.[2] For an optimal use of the delivered power, it is essential to have a good beam quality in order to concentrate the energy in the smallest area. Presently, intensities as high as 10^{21} W cm^{-2} have been reached at focus.[3] Somewhat lower intensities, in the 10^{19}–10^{20} W cm^{-2} range, are now routinely achieved in numerous laboratories either in the $\sim$30 fs/1–3 J tabletop regime[4,5] or in the $\sim$300 fs/30–400 J regime of larger-scale facilities.[6,7] The former has the advantage of allowing one to work at 10 Hz or higher repetition rate due to the relatively good thermal conductivity of broadband laser materials such as titanium doped sapphire (Ti:sapphire) crystals while the latter allows one to heat or accelerate larger volumes of matter but is limited to a single-shot regime due to Nd:glass materials used for amplification that has a lower thermal conductivity.

CPA high-power lasers are currently mainly limited in terms of achievable repetition rate and focusability. Indeed spectral distortion such as spectral gain narrowing can be nowadays pre-compensated for by spectral shaping[5,8,9] in order to produce a compressed pulse as short as possible. Moreover, higher damage-threshold dielectric-coated diffraction gratings used for temporal compression at the end of a CPA system are now available that will allow higher levels of recompressed energy.[10]

Enhancement in the repetition rate and focusability is limited by thermal load in the amplifiers. Even on a single shot, thermal load induces wave front distortions and hence reduces the beam focusability. If one tries to increase the repetition rate above the dissipation time of the thermal load, cumulative thermal load appears, the focusability worsens, and the performance of the laser further degrades. In the single-shot high-energy regime of the large-scale facilities upon which this article concentrates, thermal load originates from flashlamp-based pumping system. Since the pump spectrum is much broader than the laser material absorption

[a)]Author to whom correspondence should be addressed; electronic mail: julien.fuchs@polytechnique.fr

lines, most of the pump energy is deposited as heat, thereby inducing strong wave front distortions.[11] This is why most of the flashlamp pumped laser chains have a low repetition rate (from several tens of minutes to hours), imposed by the long laser amplifier thermalization time.

Wave front distortion is detrimental not only in reducing the peak intensity at focus but also with respect to the shot-to-shot reproducibility. Indeed changes in the spatial distribution of the amplifiers' pumping system or cumulative effects will modify the wave front distortions as a function of time, modifying the laser-matter interaction conditions throughout any particular experiment. Similar experiments carried out on different facilities will also be difficult to compare due to the different electromagnetic field configuration at focus imposed by different laser architectures and operation conditions. Wave front control and correction is therefore crucial in order to be able to focus the laser beam in an optimal, reproducible and well-defined way and hence to obtain ultimate performances for ultraintense laser facilities.

Laser wave front distortions can nowadays be compensated using wave front correction. This technique uses spatial phase modulation active devices (adaptive optics or AO) coupled to wave front measurements to lock the wave front towards a reference (usually flat). It has been initially developed in astronomy[12] and has been more recently applied to high-power lasers.[13–17] In our case, wave front correction is performed by a large aperture dielectric coated deformable mirror with a high-damage threshold that allows correction after the last amplifier, avoiding issues associated with aberrations pre-compensation.

In this article, we show that by use of an AO system that dynamically corrects the laser wave front for each shot, we are able to increase the repetition rate of a high-energy 100 TW laser while maintaining excellent focusability on every shot. The cold laser chain, where aberrations are negligible, except for defocus, has a good focusability, with a Strehl ratio[18,19] (SR) of 0.8. However, the turnaround time that is needed to dissipate the thermal load in the amplifiers and thus maintain this performance is rather long, i.e., 40 min. If the repetition rate is increased, the focusability worsens significantly and rapidly to a SR of 0.25 after five shots in 100 min. Yet, if we apply dynamic wave front correction, it is possible to reduce the turnaround time by at least a factor of 2 while maintaining a $SR > 0.75$ although the chain is not in thermal equilibrium. We also show that locking the AO system on a wave front measured after compression is necessary in order to obtain the highest intensity in the interaction area.

The article is organized as follows: after describing briefly the 100 TW laser facility at the Laboratoire pour l'Utilisation des Lasers Intenses (LULI) and its beam spatial wave front characteristics in and off thermal equilibrium, we will present our AO system and the experimental setup. Finally, we will present some results showing that a systematic active compensation of the phase distortions before each shot enables a near diffraction-limited focusability for a sequence of 100 TW shots every 20 min and an improvement of the laser chain repetition rate.

II. LULI 100 TW FACILITY, ALLOWED REPETITION RATE AND FOCUSABILITY

The LULI 100 TW facility is composed of three stages. Initially 100 fs pulses originating from a Ti:Sa "Tsunami" oscillator are stretched to 1 ns in an aberration-free Offner triplet.[20] The stretched pulses are preamplified in a Ti:Sa linear regenerative amplifier up to 1 mJ, seeding then single-pass Nd:glass rods and disk amplifiers. To cope with gain narrowing mixed glass (silicate and phosphate) is used in the rod chain to broaden the amplification bandwidth. To abate propagation effects causing intensity modulations and to suppress the scattering of energy into higher spatial frequencies by nonlinear effects causing self-focusing low pass spatial filtering and relay imaging between the amplifiers is applied. Only after the disk amplifier the beam is freely propagating to and through the compressor and towards the target chamber. Figure 1 details the layout of the rod and disk amplifiers. The beam diameter at the last amplifying stage is as large as 90 mm. A detailed description of the facility can be found in Refs. 6 and 21. The chain delivers recompressed pulses (in vacuum) of ~ 30 J in ~ 300 fs (as measured by second-order autocorrelation) at $\lambda = 1057$ nm central wavelength, resulting in laser power as high as 100 TW.

At rest, i.e., in thermal equilibrium, the chain exhibits wave front fluctuations that will eventually determine the ultimate quality of any wave front correction. These fluctuations are monitored by recording the wave front during 40 min using as a probe the 1 mJ/10 Hz beam from the regenerative Ti:sapphire preamplifier that propagates through the whole chain. Wave front sensing is achieved by a homemade achromatic three-wave lateral shearing interferometer (SID for shearing interferometer device)[22,23] that is positioned after the disk amplifier (in Fig. 1, it is designated as SID-1). Using a two-dimensional phase plate in transmission, the interferometer generates three replicas of the measured beam. After a short propagation (typically 3 mm), they interfere on a charge coupled device (CCD) camera. Three phase gradients are then extracted from the Fourier analysis of the interferogram deformations and used for the reconstruction of the spatial phase. The use of an interferometric method allows very high transverse resolution measurements, unlike the commonly used Shack-Hartmann wave front sensing technique. The latter has to balance transverse resolution (the number of microlenses) with phase measurement precision, which is linked to the number of pixels per microlens. In the case of the interferometric method, only 2 pixels per fringe are in principle necessary to recover the phase gradients through Fourier analysis. In our case, we used 4 pixels per fringes. A common limitation of interferometric methods lies in chromatic effects that blur the interferograms. In the case of the SID, the wavelength varying interfringe is exactly compensated by the angular dispersion generated by the phase grating. The achromaticity of the SID makes it well suited to either stretched or compressed large spectrum laser pulses with large bandwidth.

The observed fluctuations of the cold laser chain seldom exceed 0.2 λ. Corrections below this value will not be possible for full-energy shots even with correction. Computing

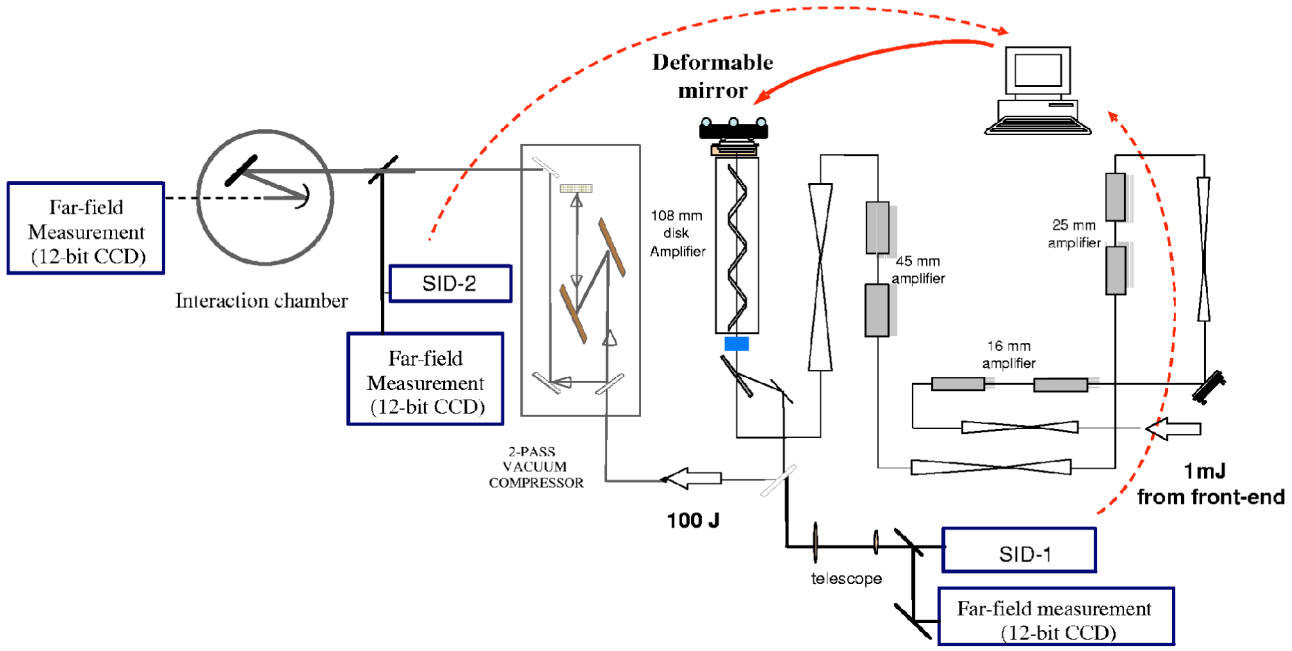

FIG. 1. (Color online) Layout of the LULI 100 TW facility amplifiers and of the implementation of the adaptive optic closed-loop system using a 100 mm deformable mirror. SID 1 and 2 are the two achromatic three-wave lateral shearing interferometers used as wave front sensors.

the Fourier transform of the wave front measurements versus time allows us to study typical periods of fluctuations. The most significant ones are every 4 and 8 min. These originate probably from air conditioning cycles in the oscillator room which modifies the output power of the regenerative amplifier pumping laser. Since the pump level is modulated in time, this induces varying temperature variations in the Ti:Sa crystal. This means that any phase measurement is valid only for about 4 min. After this delay, a drift is observed. Therefore, we know it is necessary to perform wave front correction prior to a shot within this time window in order to correct the wave front in a relevant manner for the shot.

Using the same procedure for measuring the temporal evolution of the laser wave front, we can determine the repetition rate of this facility for optimum performance at full energy. Indeed, such repetition rate is imposed by the relaxation time of the thermal load in the amplifiers. This time can be also measured by monitoring the temporal evolution of the wave front distortions after a full-energy shot. The relaxation time, i.e., the time it takes for the wave front distortion to reduce to levels observed previous to a shot, is found to be 40 min.[21]

If the CPA system operates at a higher repetition rate, the thermalization of the whole laser chain is not completed before the next shot. In this case thermal effects, accumulated from one shot to another, constantly degrade the laser beam focusability. This is illustrated in Fig. 2 where we show, measured on a 12 bit CCD camera, the focal spot in the target chamber, after pulse re-compression, for a series of five full-energy shots with a repetition rate of 20 min. In this case, note that no wave front corrector is implemented in the laser chain. The laser chain is initially cold for the first shot. Static aberrations that degrade the intrinsic focusability [see Fig. 2(a)] can be somewhat compensated by the off-axis parabola [see Fig. 2(b)] so that the focal spot exhibits a Strehl ratio of 0.8 with a full width at half maximum (FWHM) ~1.2 times diffraction-limited [see Fig. 2(a)]. As we continue to fire full-energy shots every 20 min, the central peak of the focal spot becomes dissymmetrical [see Fig. 2(c)]. More energy is spread in a large area around the central peak and the focal spot quality is strongly degraded. For the fifth shot, note that the central peak of the focal point stretches from 5 to more than 10 μm. The wave front becomes predominately aber-

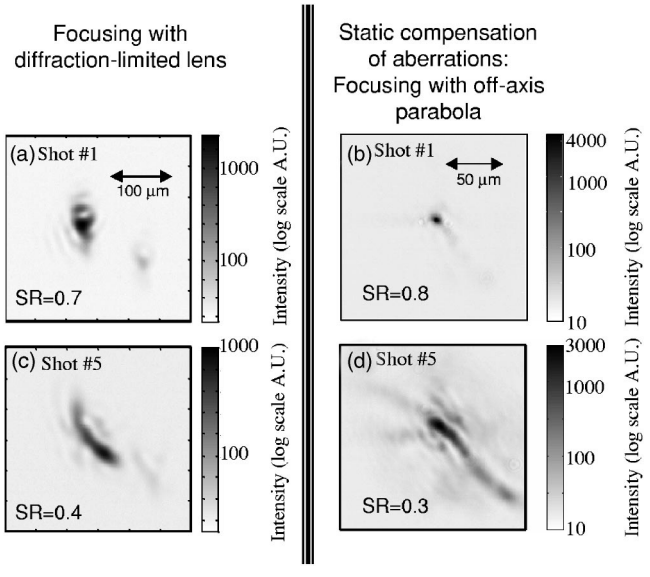

FIG. 2. Measured focal spot after pulse compression during a sequence of full-energy shots with a repetition rate of 20 min. The focusing is done either with an $f=1200$ mm diffraction-limited lens, positioned after a leak through a mirror, to test the intrinsic focusability (left) or with an $f/4.5$ off-axis parabola that is set to compensate statically the aberrations (right). (a) and (c) First shot when the chain is cool, (b) and (d) fifth shot with growing cumulative thermal effects. The spot in the lower right of (a) and (b) is due to a reflection in the optics. Strehl ratio (SR) is as indicated.

rated by thermal lens effects and astigmatism originating from thermal birefrigence. Static partial compensation of the aberrations is not enough [see Fig. 2(d)] to maintain the focusability since the aberrations are cumulative. Dynamic compensation is needed.

III. ADAPTIVE OPTICS LOOP AND EXPERIMENTAL SETUP

The closed-loop adaptive optic (AO) system we implemented on the LULI 100 TW chain for dynamic compensation of the aberrations is composed of three elements: the shearing interferometer (SID) wave front sensor mentioned above, a 100-mm-diam dielectric coated deformable mirror and a home-designed computer-based convergence loop.

The SID is a preferred sensor since it exhibits several interesting features compared to a Shack-Hartmann wave front sensor: wide achromaticity, high resolution and tunable sensitivity. Since the SID aperture (15 mm) is much smaller than the one of the laser beam, a telescope is used to down collimate the beam in the SID. For generating a flat wave front on the sensor as a reference for the adaptive optic closed loop, a pinhole with a diameter smaller than the diffraction limit can be positioned in the focal plane of the telescope.

The deformable mirror (DM) was developed by the Adaptive Optics for Industrial & Medical Applications Group in Moscow, based on bi-morph technology.[24] Two pieces of piezoelectric ceramics are glued to the back of a thin (3 mm) glass substrate. High reflectivity and damage threshold are achieved by coating this substrate with multidielectric stack. The first piezo element covers the whole surface ($\Phi = 100$ mm) and corrects global defocus. The other 30 individual electrodes are spatially distributed in three concentric rings around the beam center (with outer diameter $\Phi = 42, 73, 98$ mm). The electrode pattern allows 30 independent wave front correction channels for low order aberration correction with strokes of ± 5 μm. Applying a voltage to each electrode changes the mirror local radius of curvature. The dielectric reflective coating meets our requirements of high damage threshold (>3 GW cm^{-2} in $\Delta t = 1$ ns). The large aperture of this DM and its high damage threshold allows positioning it downstream in the chain, i.e., as the double-pass reflector of the final disk amplifier as shown in Fig. 1. This eliminates concerns associated with having a phase corrector positioned upstream.[14,15] i.e., the need to precompensate the aberrations induced along propagation in the amplifiers and thus to have to increase the diameter of the spatial filter pinholes, which induces noise at focus. Since the DM is close to a 130 mm Faraday rotator and a 108 mm disk amplifier, we checked that it is insensitive to electric and magnetic noise from a shot. In order to have an optimum correction capability, the laser beam diameter should be 20% smaller than the mirror aperture.[26] Thus we apodized the laser beam to 80 mm in the output of the last spatial filter positioned before the disk amplifier (see Fig. 1).[25]

The convergence loop is performed as follows:[26,27] the difference between the measured phase and the flat phase reference is used as the error signal in order to feed the loop back. Note that the natural very high resolution of the wave front phase map generated by the SID is decreased to fit the number of actuators; for this purpose each point in the map is averaged over 5×5 pixels. The advantage of such high resolution is first the ability to average the measurement noise and second to control with a high accuracy and level of details the wave front quality at the end of the convergence. The feedback loop basic assumption is that the induced wave front variations are linear with respect to the voltages applied on the piezoelectric actuators. Under this hypothesis, the feedback is done by inverting the matrix which links the phase maps to the set of 31 voltages to be applied. We use a pre-defined voltage applied one by one on all these 31 electrodes to determine the response matrix. More details on the convergence loop algorithm are given in Ref. 26. The adaptive optic loop usually converges in two or three iterations. The additional iterations correct the residual phase distortion due to the mirror response nonlinearities, in particular the hysterisis of the piezoelectric pieces. For each shot we record the interferogram issued by the SID, the reconstructed phase, the near-field intensity distribution and the focal spot. This allows quantifying the AO convergence loop performance.

As shown in Fig. 1, in order to evaluate the importance of wave front degradation induced by the large optics inside the compressor such as diffraction gratings, we have implemented two wave front sensors, one before and one after the compressor. The closed loop is then performed using either one of the sensors in feeding the convergence. The first sensor is placed behind the exit mirror of the laser chain. The about 2% leak of this mirror is used for wave front measurement of CPA beam before compression. To optimize the wave front correction, the deformable mirror is imaged on the wave front sensor's entrance pupil. Thus the plane in which phase is calculated images the DM plane. The second sensor is located after the compressor, also behind a leakage mirror. Since there is no image relay after the last disk amplifier, it was not possible here to image the DM plane on the sensor. Thus, the sensor images a plane between the two gratings inside the compressor. Additional attenuation of the beam before the sensor is provided for the high-energy shots.

IV. RESULTS

A. Wave front correction before compression

Similarly as in Sec. II, we have carried out a sequence of full-energy shots every 20 min., so that the laser was away from thermal equilibrium, with the adaptive optic system being activated. Before each shot, even the first one when the chain is cold, the low-energy 10 Hz beam of the regenerative amplifier that propagates through the whole optical chain is again used to investigate the spatial phase distortion. The loop converges towards the recorded flat reference wave front (using SID-1). Phase correction is performed several seconds before each shot in order to avoid deviation of the phase. Figs. 3(a) and 3(b) show that this scheme allows one indeed to provide compensation for the cumulative thermal distortions. After correction, the wave front is repeatedly flattened to the fluctuation level, i.e., 0.15 λ PtV and

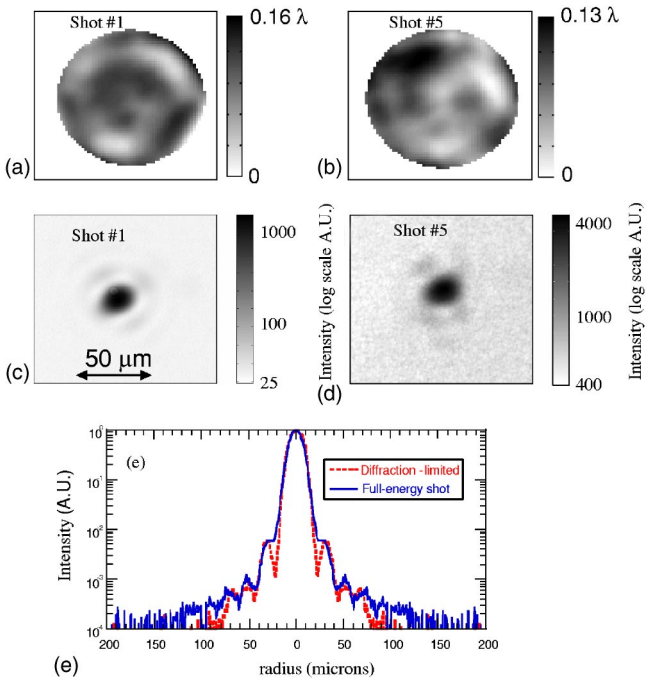

FIG. 3. (Color online) (a,b) Phase maps and (c,d) measured focal spot, recorded before compression, after convergence for the first and the fifth shot in a sequence of full-energy shots every 20 min. Wave front correction is applied with the SID-1 used as reference. (e) Azimuthally averaged profile of the focal spot for the fifth shot (solid line) and diffraction-limited Airy profile assuming a perfect focusing optics (dashed line). The SR of the actual spot is >0.9.

0.03 λ rms typically, for the all the shots throughout the sequence.

1. Observation of the focal spot before compression

The performance of the AO system is not only determined by the final phase maps but also by the intensity distribution in a focal plane that is equivalent to the one imaged by the wave front sensor, i.e., a plane before pulse recompression. Note that in this first case the far-field pattern is not influenced by the aberrations due to transport optics and compressor. The spot at the focus of a diffraction-limited $f=1200$ mm focal length lens is imaged using a microscope objective on a 12 bit CCD. As shown in Figs. 3(c) and 3(d), the focal spots before compression are nearly diffraction limited over a series of shots with a $SR>0.9$. This is expected since the plane of observation is equivalent to the one where the phase maps are observed to be nearly flat. The focusability degradation from shot to shot illustrated in Fig. 2 is cancelled out by dynamically correcting the wave front before each shot every 20 min. An excellent focal spot reproducibility between the first full-energy shot and the fifth one is observed.

2. Observation of the focal spot after compression

The compression and focusing optics degrades the excellent focusability observed before compression. We now investigate the focal spot at the center of the target chamber, in the same correction conditions as in the previous paragraph, that is with phase measurement before compression. As in Sec. II, we observe far-field patterns generated either by a

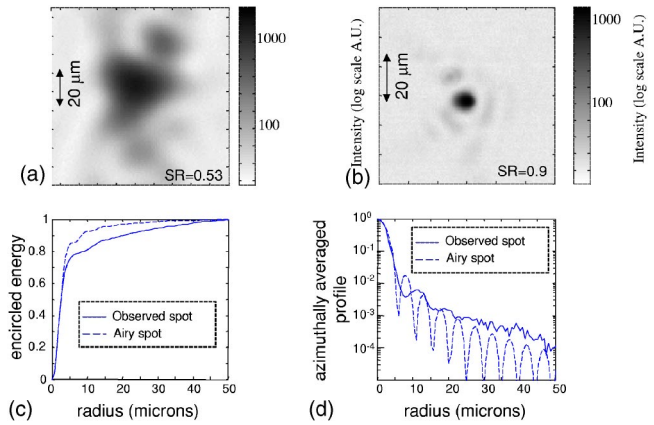

FIG. 4. (Color online) (a) Measured focal spot after pulse compression, at the center of the target chamber. This corresponds to the fifth shot of a sequence of full-energy shots every 20 min. Wave front correction is applied with the SID-1 as a reference. The focusing is done with an $f=1200$ mm diffraction-limited lens, positioned after a leak through a mirror, to test the intrinsic focusability. (b) Same but the focusing is done with an $f/4.5$ off-axis parabola. (c) Encircled energy for the spot shown in (b) superposed with the same for the Airy spot that would be produced by a perfect parabola. (d) Azimuthally averaged profile for the spot shown in (b) and also for a perfect Airy spot.

long focal length lens, to measure the intrinsic focusability, or by an $f/4.5$ off-axis parabola, to measure a realistic full-power focal spot, as used in experiments. The lens-focusing system is positioned after a leakage to avoid nonlinear effects in the lens when firing at full-energy in the compressor (see Fig. 1). Note that in Fig. 4 we only show the fifth shot in a sequence, the others being similar given that the results of the AO loop are well reproducible, as has been shown in the previous section.

Compared to Fig. 3, one observes a lower intrinsic focusability than what is measured before compression [see Fig. 4(a)]. This is due to the aberrations in the compressor and the target area, i.e., after the convergence is performed: $\sim 1\lambda$ of PtV is measured with SID-2. These probably correspond to distortions of the large optical components such as the 40×20 cm gratings, the large aperture plates and mirrors. In order to eliminate concerns regarding residual misalignment of the compressor that would produce wavelength related wave front errors, the compressor was aligned with care before the experiment, including verification by interferometric field autocorrelation.[28]

The intrinsic focusability is also relatively lower in this case compared to the situation where there was no DM implemented and the chain was cold [see Fig. 2(a)]. However, the residual aberrations that result from the convolution between the incident wave front and the wave front defaults of the optics are different in the two cases. Fortunately, the static aberrations introduced by the large optics in the compressor and the target area can be compensated by the off-axis parabola, as evidenced by Fig. 4(b). Aligning the parabola using the low-energy, 10 Hz beam that is corrected before compression, we obtain a good quality beam both at 10 Hz and for full-power shots. In a series of full-energy shots every 20 min, the SR of the observed spot varies between 0.9 and 0.8, depending on the residual wave front fluctuations after correction, when dynamic wave front cor-

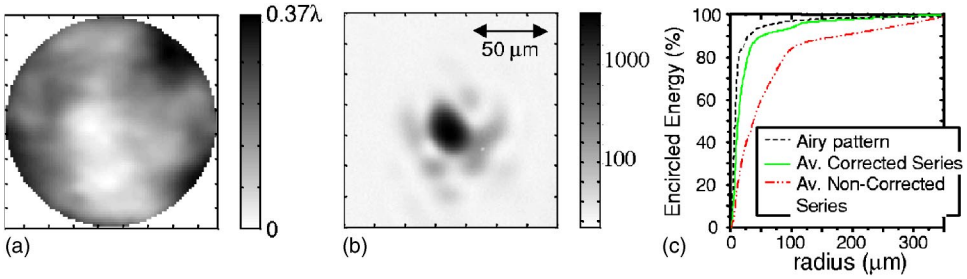

FIG. 5. (Color online) (a) Phase map, recorded after compression, after convergence for the fifth shot in a sequence of full-energy shots every 20 min. Wave front correction is applied with the SID-2 as a reference. (b) Recorded focal spot for the same shot and after pulse compression, at the center of the target chamber. The SR is 0.9. (d) Encircled energy as a function of radius for the average focal spot of the series of five corrected shots (solid line), for the average focal spot of the series of five uncorrected shots as shown in Fig. 2 (dash-dot line) and for the Airy profile assuming a perfect focusing optics (dashed line).

rection is applied on the chain away from thermal equilibrium. More than 70% of the energy is contained in the central peak. The FWHM of the focal spot is 4.9 μm. This performance is to compare to a SR of $\sim$0.25 without correction. This represents an improvement of a factor >3 in the peak intensity at a level of $>1.5\times10^{20}$ W cm^{-2}, and, most important, allows one to keep a constant focal spot shape which is crucial for some physical phenomena.[29]

B. Wave front correction after compression

Performing wave front correction after compression improves the intrinsic focusability significantly. This is made by locking the convergence loop on SID-2 that is positioned after the pulse recompression (see Fig. 1) instead of SID-1. However, since unlike SID-1 this sensor does not image the DM plane, direct convergence proves to be difficult. Indeed, when we start a convergence sequence, the aberration level can be quite high and the lack of imaging can induce errors that are important enough to make the loop diverge. This is why we first perform a convergence using SID-1. Then, once the absolute level of aberrations as seen after compression is already low, we switch to feeding the loop with the phase measured by SID-2. This way convergence is assured. To test the improvement on the intrinsic focusability, we only image the focal spot of a long-focal length (1.2 m), diffraction-limited lens. As in the previous sections, to test the loop, we fired a sequence of five full-energy shots with a repetition rate of (20 min).

The improvement is significant, as shown in Fig. 5: the wave front PtV is reduced compared to when the correction is performed with SID-1 and the SR of the focal spot evolves around 0.75 and can reach 0.9, still depending on the residual wave front fluctuations after correction. This variation, higher than when using SID-1, may originate from the lesser stability of the loop that uses SID-2. The corrected wave front PtV during the shot varies between 0.3 and 0.6 λ, whereas when correcting with SID-1 it was $\sim$0.15λ and stable. The result of this convergence is to compare to Fig. 4(a) when correction was provided by SID-1 (SR=0.5) and to Fig. 2 without correction (SR=0.25 after five shots). If we average the encircled energy curves [see Fig. 5(c)], we find that for noncorrected shots [see Fig. 2] less than 30% of the energy was contained in the first Airy disk. However, the focusing pattern in far field can reliably be reproduced for each shot with dynamic wave front correction. More than 70% of the energy was concentrated in the Airy disk for corrected shots. With this correction, if focused by an $f/3$, respectively $f/1$, off-axis parabola, the peak intensity could be as high as 3.8×10^{20} W cm^{-2}, respectively 3.4×10^{21} W cm^{-2}.

The reduction of the repetition rate to 20 min in the present study is limited by the induced birefringence in the amplifiers. Since the laser chain outputs 100 J and since only 40 J at maximum in p polarization can be directed in the pulse compressor, due to the grating damage threshold, it is foreseeable to further increase the repetition rate: the limit would then be determined by the amount of birefringence that is acceptable while still having 40 J in p polarization in the output of the amplifiers. Future plans also include applying the techniques developed in the present study to the currently developed PetaWatt facilities at LULI[30] and GSI which plan to deliver 500 J in 500 fs.

ACKNOWLEDGMENTS

The authors acknowledge the expert support of C. Le-Bris and C. Félix of the LULI laser team. This work was supported by Grant No. E1127 from Région Ile-de-France, European "Adaptool" RTD Contract No. HPRI-CT-1999-50012, corporate support of General Atomics and UNR Grant No. DE-FC08-01NV14050.

[1] C. Joshi and P. Corkum, Phys. Today **48**, 36 (1995); G. Mourou, C. Barty, and M. Perry, *ibid.* **51**, 22 (1998); C. Joshi and T. Katsouleas, *ibid.* **56**, 47 (2003).
[2] D. Strickland and G. Mourou, Opt. Commun. **56**, 219 (1985).
[3] J. D. Bonlie *et al.*, Appl. Phys. Lett. **70** [Suppl.], S155 (2000).
[4] K. Yamakawa *et al.*, Opt. Lett. **23**, 1468 (1998).
[5] M. Pittman *et al.*, Appl. Phys. B: Lasers Opt. **74**, 529 (2002).
[6] J. P. Zou *et al.*, Proc. SPIE **3492**, 94 (1999).
[7] N. Blanchot *et al.*, Opt. Lett. **20**, 395 (1995); M. Perry *et al.*, *ibid.* **24**, 160 (1999).
[8] Y. H. Cha, Y. I. Kang, and C. H. Nam, J. Opt. Soc. Am. B **16**, 1220 (1999).
[9] F. Verluise, V. Laude, Z. Cheng, Ch. Spielmann, and P. Tournois, Opt. Lett. **25**, 575 (2000).
[10] A. Reichart *et al.*, Proc. SPIE **4347**, 521 (2001).
[11] W. Koechner, *Solid State Laser Engineering* (Springer, Berlin, 1999), Chap. 7; D. C. Brown, *High-Peak-Power Nd:Glass Laser Systems*, Springer Series in Optical Sciences, (Springer, Berlin, 1981), Vol. 25.
[12] F. Roddier, *Adaptive Optics in Astronomy* (Cambridge University Press, Cambridge, 1999).
[13] F. Druon, G. Chériaux, J. Faure, J. Nees, M. Nantel, A. Maksimchuk,

G. Mourou, J.-C. Chanteloup, and G. Vdovin, Opt. Lett. **23**, 1043 (1998).
[14] D. M. Pennington, C. G. Brown, T. E. Cowan, S. P. Hatchett, E. Henry, S. Herman, M. Kartz, M. Key, J. Koch, A. J. MacKinnon, M. D. Perry, T. W. Phillips, M. Roth, T. C. Sangster, M. Singh, R. A. Snavely, M. Stoyer, B. C. Stuart, and S. C. Wilks, IEEE J. Sel. Top. Quantum Electron. **6**, 676 (2000).
[15] J.-C. Chanteloup, H. Baldis, A. Migus, G. Mourou, B. Loiseaux, and J.-P. Huignard, Opt. Lett. **23**, 475 (1998).
[16] H. Baumhacker, G. Pretzler, K. J. Witte, M. Hegelich, M. Kaluza, S. Karsch, A. Kudryashov, V. Samarkin, and A. Roukossouev, Opt. Lett. **27**, 1570 (2002).
[17] C. Haefner, PhD dissertation, University of Heidelberg, Germany, 2003, http://www.ub.uni-heidelberg.de/archiv/4548
[18] K. Strehl, Z. Instrumentenkd. **22**, 213 (1902). It is the ratio of the peak intensity at the focus of the beam with the given (distorted) wave front and its near-field intensity profile, to that of the same near-field intensity distribution with a flat wave front.
[19] The SR is measured through direct imaging focal spot at full power at different points along the chain, including the target chamber center. Therefore it includes any potential default originating from the focusing optics used, on the contrary of methods simulating the focal spot from phase measurements only.
[20] G. Chériaux *et al.*, Opt. Lett. **21**, 414 (1996).
[21] J. P. Zou *et al.*, Proc. SPIE **5137**, 188 (2003).
[22] J. Primot and L. Sogno, J. Opt. Soc. Am. A **12**, 2679 (1995).
[23] J.-C. Chanteloup, F. Druon, M. Nantel, A. Maksimchuk, and G. Mourou, Opt. Lett. **23**, 621 (1998).
[24] A. V. Kudryashov, V. B. Kulakov, Ye. V. Kotsuba, V. Ya. Panchenko, and V. I. Samarkin, Proc. SPIE **3688**, 469 (1999).
[25] This issue has been now alleviated by use of a 110-mm-diam deformable mirror that allows one to use the whole aperture (and energy) of the laser amplifiers.
[26] B. Wattellier *et al.*, J. Opt. Soc. Am. B **20**, 1632 (2003).
[27] B. Wattellier, PhD dissertation, Ecole Polytechnique, Palaiseau, France, 2001.
[28] G. Pretzler, A. Kasper, and K. J. Witte, Appl. Phys. B: Lasers Opt. **70**, 1 (2000).
[29] J. Fuchs, T. Cowan, P. Audebert, H. Ruhl, L. Gremillet, A. Kemp, M. Allen, A. Blazevic, J.-C. Gauthier, M. Geissel, M. Hegelich, S. Karsch, P. Parks, M. Roth, Y. Sentoku, R. Stephens, and E. M. Campbell, Phys. Rev. Lett. **91**, 255002 (2003).
[30] C. Le Blanc *et al.*, in *Inertial Fusion Science and Applications 2003* (American Nuclear Society, La Grange Park, IL, 2004), p. 608.